IEEE Access
Multidisciplinary | Rapid Review | Open Access Journal

Received May 29, 2020, accepted June 15, 2020, date of publication June 30, 2020, date of current version July 20, 2020.

Digital Object Identifier 10.1109/ACCESS.2020.3005906

Comparing Test-Retest Reliability of Entropy Methods: Complexity Analysis of Resting-State fMRI

YAN NIU[1], JIE SUN[1], BIN WANG[1], WAQAR HUSSAIN[1], CHANJUAN FAN[1], RUI CAO[2], MENGNI ZHOU[3], AND JIE XIANG[1]

[1]College of Information and Computer, Taiyuan University of Technology, Taiyuan 030024, China
[2]College of Software, Taiyuan University of Technology, Taiyuan 030024, China
[3]Graduate School of Interdisciplinary Science and Engineering in Health Systems, Okayama University, Okayama 700-8530, Japan

Corresponding author: Jie Xiang (xiangjie@tyut.edu.cn)

This work was supported in part by the National Natural Science Foundation of China under Grant 61503272, Grant 61305142, Grant 61373101, and Grant 61873178, in part by the Natural Science Foundation of Shanxi under Grant 2015021090, in part by the China Postdoctoral Science Foundation under Grant 2016M601287, in part by the Shanxi Provincial Innovation Foundation for Outstanding Doctoral Students under Grant 2019BY032, and in part by the Shanxi Provincial International Cooperation Foundation under Grant 201803D421047.

ABSTRACT In recent years, there has been growing interest in studying the complexity of resting-state functional magnetic resonance imaging (rs-fMRI) brain signals. As one of the most commonly used complexity methods, entropy measures have been used to quantitatively characterize abnormal brain activity in aged individuals and patients with psychopathic and neurological disorders, and most studies have analyzed brain signals from a single channel. The widely used entropy methods include approximate entropy (AE), sample entropy (SE), permutation entropy (PE), and fuzzy entropy (FE). However, the test-retest reliability of different entropy methods remains to be explored. In this study, we investigated the distribution and test-retest reliability of four entropy measures and a new entropy algorithm we proposed, permutation fuzzy entropy (PFE), in three independent data sets at three levels, i.e., based on voxels, brain regions, and functional networks. Our results showed that analyzing fMRI signals with entropy showed strong tissue sensitivity. The highest reliability was achieved with PFE, and PE and FE were superior to AE and SE at all three levels. The percentage of nodes with good to excellent reliability in PFE, PE, FE, SE and AE was 94.31%, 52.65%, 18.56%, 11.36% and 0.76%, respectively. PFE and PE showed fair to good reliability in the visual network, auditory network, default-mode network, etc. In conclusion, characterizing brain entropy may provide an informative tool to assess the complexity of brain functions. Our results suggested that PFE and PE had better reliability and reflected more topological information related to normal and disordered functioning of the human brain.

INDEX TERMS Functional magnetic resonance imaging (fMRI), test-retest reliability, permutation fuzzy entropy (PFE), permutation entropy (PE).

I. INTRODUCTION

The human brain is a nonlinear and complex system. There has been increasing interest in analyzing the complexity of brain signals with technologies such as electroencephalogram (EEG) [1], magnetoencephalogram (MEG) [2], and functional magnetic resonance imaging (fMRI) [3]. Blood oxygenation level-dependent (BOLD) fMRI is a powerful noninvasive tool for whole-brain imaging [4].

Resting-state fMRI (rs-fMRI) can reflect the spontaneous neural activity of the human brain and can be used to study the intrinsic function of the human brain. In recent years, there has been growing interest in studying the complexity of rs-fMRI brain signals [5].

There are numerous complexity methods, such as the Lyapunov exponent, correlation dimension, Lempel-Ziv

The associate editor coordinating the review of this manuscript and approving it for publication was Sudipta Roy.

complexity, Hurst exponent, and entropy [6], [7]. These methods use the time series of brain signals to construct a multidimensional state space to reflect different complex states of the brain [8]. In addition, these methods evaluate the complexity of the signal based on its unpredictability: irregular signals are more complex than regular signals. Among these methods, due to its simple algorithm, the small amount of data required and the strong antinoise ability in calculation, entropy is one of the most widely used complexity methods for evaluating the dynamic characteristics of brain signals [9]. The lower the entropy value is, the lower the complexity of the signal. This method is robust to noise and artifacts and can be used to analyze biological data. Entropy methods have been widely used in physiological signal analysis, including approximate entropy (AE) [10], sample entropy (SE) [11], fuzzy entropy (FE) [12], and permutation entropy (PE) [13].

SE, as proposed by Richman and Moorman, is an improved version of Pincus's AE and aimed to overcome the limitations of AE and reduce statistical bias [14]. FE is an improvement over the AE and SE algorithms. PE, another widely used entropy measure, is a novel method developed by Bandt to characterize the complexity of time series [13]. PE is suitable for capturing the complex dynamics and rich time structure embedded in biological systems. Considering that brain signals are very susceptible to noise during the acquisition process, the antinoise performance of entropy is significant. Permutation fuzzy entropy (PFE), a new index we proposed, had better antinoise performance and detection performance than PE and FE [15].

In recent years, entropy has been widely used on EEG and MEG signals, but relatively few studies have employed this approach for fMRI. Moses O. Sokunbi *et al.* conducted multiple fMRI signal studies using different measures of entropy: using AE to study individual differences in cognitive performance in an elderly population, the results showed that higher regional signal entropy was associated with better cognitive performance [16]; SE was used to study the complexity of fMRI signals in the brain of schizophrenia patients, and it was found that the complexity in the signals from these patients was higher than that of healthy controls at the global and local levels [17]; they also used SE to analyze the fMRI signals from patients with attention-deficit/hyperactivity disorder and found that the entropy values of the fMRI signal from the whole brain of these patients were lower than those of the controls [18]; furthermore, the analysis of the complexity of fMRI signals from 41 healthy adults (41 males, 19 to 85 years old) showed that brain entropy values at the global and local levels were negatively correlated with age [19]. Lin *et al.* used SE to explore changes in the entropy of fMRI signals from the brains of patients with depression and found that compared with normal controls, patients with depression showed reduced entropy in the medial orbitofrontal cortex and cingulate cortex but increased brain signal complexity in the motor cortex, which revealed the intrinsic network dynamics that have been widely used in the study of the mechanisms underlying mental disorders [20]. These studies showed that entropy measures can both analyze the temporal changes in fMRI signals and locate the relevant brain space.

Studies on fMRI showed that the change in entropy value is related to disease states and can also be used to study the internal mechanism of the normal human brain. However, to determine the entropy method that most reliably reflects the complexity of biological systems, few studies have systematically analyzed the test-retest reliability of these entropy methods applied to fMRI signals.

In this study, the distribution and test-retest performance of five entropy methods (AE, SE, PE, FE and PFE) were compared. We performed complexity analysis at three levels—based on voxels, brain regions, and brain networks—using three rs-fMRI data sets from healthy young people. Our research aims to provide a reference for researchers who use entropy to explore the complexity of fMRI signals.

II. MATERIALS AND METHODS

A. SUBJECTS

In this experiment, three published rs-fMRI test-retest data sets were used. The first data set is from IPCAS (http://dx.doi.org/10.15387/fcp_indi.corr.ipcas1), which contains data from 30 right-handed healthy college students (average age: 20.93 $\pm$ 1.72; 9 males). One subject lacked information on three rs-fMRI scans, so we selected 29 subjects for the test-retest study (8 males).

The second set of experimental data was from the NITRC public database (http://www.nitrc.org/projects /nyu_trt/), in particular, the NYU data set, which includes 25 right-handed volunteers (average age: 30.7 $\pm$ 8.8; 9 males), and each subject was scanned three times.

The third set of data, IBA (http://dx.doi.org/10.15387 /fcp_indi.corr.ibatrt1), contains 36 subjects (mean age: 27.3 $\pm$ 7.75; 18 males), and each subject underwent two rs-fMRI scans.

B. EXPERIMENTAL PROCEDURE AND DATA ACQUISITION

The experimental procedure is shown in Fig. 1. During the resting-state scan, a fixation cross was presented to the first group of 29 subjects, and the subjects were instructed to rest while focusing on the fixation cross. Three resting-state scans were obtained for each subject using a Siemens 3T scanner. The researchers acquired echo-planar imaging (EPI) functional volumes of each scan (repetition time (TR) = 2500 ms; echo time (TE) = 30 ms; flip angle (FA) = 90°, number of slices = 32, matrix = 64 $\times$ 64; field of view (FOV) = 256 mm, acquisition voxel size = 3 $\times$ 3 $\times$ 3 mm^3) and structural MRI data using sagittal T1-weighted magnetization prepared rapid gradient echo (MPRAGE) sequences (TR = 2530 ms; TE = 2.51 ms; inversion time = 1100 ms; FA = 7°; number of slices = 128; FOV = 256 mm). The mean interval between scans 1 and 2 was 29 minutes, and the mean interval to scan 3 was 5-24 days.

The second group of 25 subjects were asked to relax and keep their eyes open during the scan. Each subject underwent

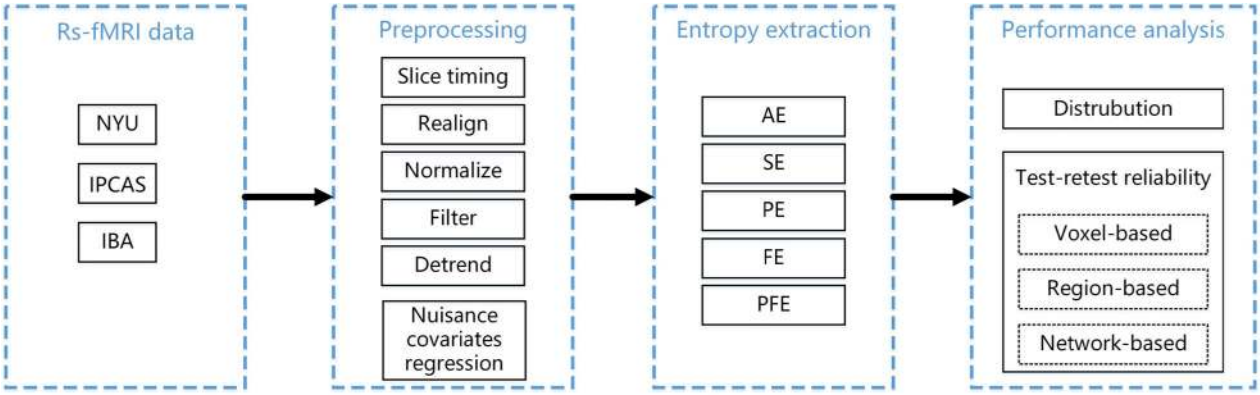

FIGURE 1. The total experimental procedure.

three resting-state scans using the Siemens Allegra 3T scanner. Each scan consisted of 197 contiguous EPI functional volumes (scanning parameters: TR = 2000 ms; TE = 25 ms; FA = 90°; number of slices = 39; matrix = 64 × 64; FOV = 192 mm) and the high-resolution T1-weighted MPRAGE sequence (TR = 2500 ms; TE = 4.35 ms; inversion time = 900 ms; FA = 8°; number of layers = 176; FOV = 256 mm). Scans 2 and 3 were performed 5-16 months after scan 1 (average 11 ± 4 months), and the interval between the second scan and the third scan was 45 minutes.

The 36 subjects in the third group were asked to relax and open their eyes during the scanning process. Using a Siemens 3T scanner and EPI technology, each participant was scanned in the resting state (scanning parameters: TR = 1750 ms; TE = 30 ms; FA = 90°; number of layers = 29 layers; matrix = 64 × 64; FOV = 220 mm; data collected at 343 time points) and with a high-resolution T1-weighted MPRAGE sequence (TR = 2600 ms; TE = 3.02 ms; inversion time = 900 ms; FA = 8°; number of layers = 176; FOV = 256 mm). Each of these scans was performed at an interval of 51-183 days.

C. SIGNAL PREPROCESSING

The Data Processing Assistant for Resting-State fMRI (DPARSF v2.3) software package was used, which is based on two software packages—Statistical Parametric Mapping 8 (SPM 8) and RS-fMRI Data Analysis Toolkit 1.8 (REST 1.8) [21]—and the images were analyzed on the MATLAB 2014a platform [22]. The preprocessing process for each subject was as follows: removal of the first 10 time points; slice-timing correction; head movement correction; spatial normalization based on EPI template; resampling of voxel size to 3 mm × 3 mm × 3 mm; bandpass filtering to reduce the impact of low-frequency drift and high-frequency physiological noise; detrending; removal of linear drift; removal of the effect of nuisance covariates including head motion parameters, white matter signal and cerebrospinal fluid signal.

D. ENTROPY ALGORITHMS

To compare the test-retest reliability of entropy methods, we applied entropy to investigate the complexity of rs-fMRI signals. Entropy is defined as the rate of new information generation, which measures the probability of generating a new pattern in the signal. The greater the probability of generating a new pattern that there is, the greater the signal complexity. This value was calculated with the following formula:

$$H = -\sum_{i=1}^{n} p_i \log p_i \tag{1}$$

In the formula, P_i represents the probability of the i-th discrete state.

Here, five entropy algorithms were applied as complexity estimators of rs-fMRI signals: (1) Approximate entropy (AE) is roughly equivalent to the mean value of the logarithmic conditional probability of the new state appearing when the dimension changes, and it has certain value in measuring the complexity of the time series. (2) Sample entropy (SE) is an improvement relative to the AE algorithm in that SE calculates the logarithm of the sum and aims to reduce the error of the AE, which is more closely consistent with the known random part. (3) Fuzzy entropy (FE) adds a fuzzy function to the comparison of continuous point vectors and generalizes these vectors to reduce the impact of measurement drift. (4) Permutation entropy (PE) uses the shape of neighboring points to evaluate complexity based on permutation patterns, and it has good computing performance for analyses of any real-world data. (5) Permutation fuzzy entropy (PFE) is calculated by first conducting permutations based on the original time series. After data preprocessing, entropy was computed based on the time course of every voxel in the brain.

1) APPROXIMATE ENTROPY

Step 1: Given a time series of N lengths:

$$\mathrm{X} = \{\mathrm{x}(1), \mathrm{x}(2), \cdots \mathrm{x}(\mathrm{N})\} \tag{2}$$

Step 2: Reconstructed vector with m dimensions represents the value of m continuous x starting at point i:

$$\mathrm{X_i} = \{\mathrm{x(i)},\mathrm{x(i+1)}, \cdots \mathrm{x(i+m-1)}\}, \quad 1 \le \mathrm{i} \le \mathrm{N-m+1} \tag{3}$$

Step 3: The distance d_{ij}^{m} between vectors X_i^m and $X_j(j = 1, 2 \cdots N - m + 1, j \neq i)$ is defined as the largest difference between corresponding elements and the maximum absolute difference as its corresponding scalar component:

$$d_{ij} = \max |x(i + j) - x(j + k)|, \quad k = 0,1, \cdots m - 1 \tag{4}$$

Step 4: Given threshold r, count the number of distances between the vector X_i and all vectors that are less than the threshold for any given vector $d_{ij} \leq r \times SD$(SD is the standard deviation of the original one-dimensional time series), and calculate its vector and total n-m + 1 ratio, recorded as $C_i^m(i)$; take the logarithm; and then find its average value, recorded as $\phi^m(r)$. The calculation formula is as follows:

$$\phi^m(r) = \frac{1}{N - m + 1} \sum_{i=1}^{N-m+1} \ln C_i^m(r) \tag{5}$$

Step 5: Increase the reconstruction dimension from m to m + 1, and calculate $\phi^m(t)$. For finite time series, approximate entropy is obtained:

$$AE(N, m, r) = \phi^m(r) - \phi^{m+1}(r) \tag{6}$$

Among the parameters in the algorithm, N represents the length of time series, m is phase space dimension, and r is similar tolerance.

2) SAMPLE ENTROPY

Step 1: Given a time series of N lengths:

$$X = \{x(1), x(2), \cdots x(N)\} \tag{7}$$

Step 2: Reconstructed vector with m dimensions:

$$X_i^m = \{x(i), x(i + 1), \cdots x(i + m - 1)\}, \quad 1 \leq i \leq N - m + 1 \tag{8}$$

Step 3: The distance d_{ij}^m between vectors X_i^m and X_j^m is defined as the largest difference between corresponding elements.

$$d_{ij}^m = d[X_i^m, X_j^m] = \max |x(i + k) - x(j + k)|, \quad k = 0, 1, \cdots m - 1 \tag{9}$$

Step 4: Given the value r similar tolerance, the distance between vectors is calculated as the maximum absolute distance between their corresponding scalar elements. Count the number of distances less than r and normalize them as $B_r^m(i)$:

$$B_r^m(i) = \frac{1}{N - m - 1} \sum_{j=1, j\neq i}^{N-m} \Theta(d_{ij}^m - r), \Theta(z) = \begin{cases} 0, & z < 0 \\ 1, & z \geq 0 \end{cases} \tag{10}$$

Step 5: Average all i:

$$B_r^m = \frac{1}{N - m} \sum_{i=1}^{N-m} B_r^m(i) \tag{11}$$

Step 6: Increase the reconstruction dimension from m to m + 1, and calculate B_r^{m+1}. When the length N of series U is finite, the estimated value of the corresponding sample entropy is shown as

$$SE(N, m, r) = -\ln(B_r^{m+1}/B_r^m) \tag{12}$$

Among the parameters in the algorithm, N represents the time series length, m is the phase space dimension, and r is similar tolerance. The more complex the time series, the greater the corresponding sample entropy.

3) FUZZY ENTROPY

Step 1: Given a time series of N lengths:

$$X = \{x(1), x(2), \cdots x(N)\} \tag{13}$$

Step 2: Phase space reconstruction:

$$X_i^m = \{x(i), x(i + 1), \cdots x(i + m - 1)\} - x_0(i), \quad 1 \leq i \leq N - m + 1 \tag{14}$$

$$x_0(i) = \frac{1}{m} \sum_{j=0}^{m-1} u(i + j) \tag{15}$$

Step 3: The distance d_{ij}^m between vectors X_i^m and X_j^m is defined as the largest difference between corresponding elements.

$$d_{ij}^m = d\left[X_i^m, Y_j^m\right] = \max_{k=1,2,\cdots,m} (|x(i + k - 1) - x_0(i)| - |x(j + k - 1) - x_0(j)|) \quad i, j = 1, 2, \cdots N - m + 1, j \neq i \tag{16}$$

Step 4: The distance D_{ij}^m between vectors X_i^m and X_j^m is defined using a fuzzy membership function $\mu(d_{ij}^m, n, r)$:

$$D_{ij}^m = \mu(d_{ij}^m, n, r) = \exp\left(\frac{-(d_{ij}^m)^n}{r}\right) \tag{17}$$

In this expression, the fuzzy function $\mu(d_{ij}^m, n, r)$ is an exponential function. Respectively, n and r are the width and gradient of the exponential function.

Step 5: Define function $\phi^m(r)$:

$$\phi^m(r) = \frac{1}{N - m + 1} \sum_{i=1}^{N-m+1} \left(\frac{1}{N - m} \sum_{j=1, j\neq i}^{N-m+1} D_{ij}^m\right) \tag{18}$$

Step 6: Increase the reconstruction dimension from m to m + 1, and calculate $\phi^{m+1}(r)$. When the length N of series U is finite, the estimated value of the corresponding fuzzy entropy is shown:

$$FE(N, m, r) = \ln \phi^m(r) - \ln \phi^{m+1}(r) \tag{19}$$

Among the parameters in the algorithm, N represents the time series length, m is the phase space dimension, and r is similar tolerance. Fuzzy entropy also measures the probability of the new model. The greater the probability, the greater the complexity.

4) PERMUTATION ENTROPY

Step 1: Given a time series of N lengths:

$$X = \{x(1), x(2), \cdots x(N)\} \tag{20}$$

Step 2: The pm dimensional phase space reconstruction of raw data by serial number:

$$X(i) = \left[x(i), x(i+\tau), \cdots, x(i+(pm-1)\tau)\right], \quad i = 1, 2, \cdots N-(pm-1)\tau \tag{21}$$

where pm is the embedding dimension and τ is the delay time.

Step 3: Each reconstructed component is rearranged in ascending numerical order:

$$x(i+(j_1-1)\tau) \le x(i+(j_2-1)\tau) \le \cdots \le x(i+(j_{pm}-1)) \tag{22}$$

$j_1, j_2, \cdots, j_{pm}$ represent an index of the columns of each element in the reconstructed component.

If two values are equal, for example,

$$x(i+(j_1-1)\tau) = x(i+(j_2-1)\tau) \tag{23}$$

They are ordered according to the size of the j1, j2 value, and when $j1 < j2$:

$$x(i+(j_1-1)\tau) < x(i+(j_2-1)\tau) \tag{24}$$

Step 4: We can obtain a set of symbol sequences according to the raw data from the reconstructed matrix of any time series, where the symbol sequences is as follows:

$$s(g) = (j_1, j_2, \cdots, j_{pm}), \quad g = 1, 2, \cdots, k, k \le pm! \tag{25}$$

Step 5: There are pm! possible scenarios for different symbol sequences obtained by pm dimension mapping, and s (g) is only one of them. Calculating the probability of occurrence of various permutations $P_1, P_2, \cdots, P_k$, the permutation entropy is defined as

$$PE(N, pm, \tau) = -\sum_{j=1}^{k} P_j \ln P_j \tag{26}$$

Three parameter values must be considered and set when calculating PE: length of time series N, embedding dimension pm, and time delay τ. PE size represents the random degree of the time series, and a smaller value indicates that the time series is more regular; otherwise, the time series is more random.

5) PERMUTATION FUZZY ENTROPY

The permutation fuzzy entropy is first sorted and symbolized for the original time series; then, the fuzzy entropy of the signed sequence is calculated. The permutation fuzzy entropy algorithm is as follows:

Step 1: Given a time series of N lengths:

$$X = \{x(1), x(2), \cdots x(N)\} \tag{27}$$

Step 2: The pm dimensional phase space reconstruction of raw data by serial number:

$$X(i) = \left[x(i), x(i+\tau), \cdots, x(i+(pm-1)\tau)\right], \quad i = 1, 2, \cdots N-(pm-1)\tau \tag{28}$$

where τ and pm are the embedding time delay and the permuted dimension (the number of samples included in each motif), respectively.

Step 3: The $N-(pm-1)\tau$ reconstruction components can be obtained by Step 2. Rearrange all of the elements in each of the reconstruction components in ascending order according to their numerical values. If two elements are equal, the numerical values of the next elements from their corresponding reconstruction components are used as the current comparison results for rearrangement to reflect the instant trend of the time series. If the numerical values of the next elements are still equal, the index values are used for the ascending order rearrangement. A different symbolic sequence can be obtained by extracting the indexes of all elements in their original reconstruction components. Each instance of pm! in the symbolic sequence corresponds to a value between 1 and pm!. Therefore, the original time series is converted to a new series with each element having a value between 1 and pm!:

$$Y(i), \quad 1 \le i \le N-(pm-1)\tau \tag{29}$$

Step 4: For the new sequence, the fuzzy entropy is calculated according to Formula (13) to Formula (18), and the permutation fuzzy entropy of the original sequence x (i) is obtained:

$$PFE(N, pm, \tau, m, r) = \ln \phi^m(r) - \ln \phi^{m+1}(r) \tag{30}$$

The parameter N represents the time series length, pm is the embedding dimension, τ is the delay time, m is the phase space dimension, and r is the similar tolerance.

E. PARAMETER SELECTION

This study uses three data sets to compare the test-retest performance of the five entropy methods. AE, SE, and FE need to set three parameters: N, m, and r. N is the number of time points, m specifies the dimension of the phase space, and r is the similarity tolerance. Many studies have discussed the setting of these parameters [23], [24]. The parameter m is taken as 2, and the similarity tolerance r is taken as 0.25 times the standard deviation of the original data.

The PE algorithm also involves the setting of 3 parameters: N, pm, and τ, where N is the time series, pm is the embedding dimension, and τ is the delay time. The pm value setting is based on the following considerations: when $pm < 3$, the process is meaningless because there are too few permutations and combinations; the larger the pm is, the more the algorithm time complexity will increase as a larger m corresponds to more permutations. Bandt and Pompesuggested that pm should be $3 \sim 7$ [13]; Li *et al.*, to ensure sensitivity to the transient characteristics of the system, suggested that the pm

should be a small value to reduce the time complexity of the algorithm [25]. In this study, pm was set as 4. For the time delay in the sorting and symbolization process, the value used in this study was 1. In this setting, more information can be captured in brain signals.

The PFE algorithm involves the setting of 5 parameters: N, m, r, pm, and τ. N is the original time series, m was set to 2, the similarity tolerance r was set as 0.25 times the standard derivation of the original time series, the embedding dimension pm was set as 4, and the delay time τ was set to 1.

In addition, this study involved the comparison of different entropy methods. To avoid the influence of parameter settings on the results, at the end of the experiment, we compared the test-retest performance of different entropy measures using parameters across the entire possible range.

F. TEST-RETEST RELIABILITY

The test-retest reliability evaluates the statistical stability of the index at different measurement times [26]. It comprehensively considers the changes within the individual and among different individuals, reflecting the stability and consistency of the index across time [27]. Test-retest reliability is a very important concept in various fields, including sociology, behavior, physics, biology and medicine [28]. Due to the interference of various factors on the actual measurement, it is critical to choose a reliable index. The intraclass correlation coefficient (ICC) is a commonly used reliability coefficient index to measure test-retest reliability [26]. The ICC value can be calculated according to the following formula:

$$\mathrm{ICC} = \frac{\mathrm{MS_R} - \mathrm{MS_E}}{\mathrm{MS_R} + (\mathrm{k}-1)\mathrm{MS_E}} \tag{31}$$

$\mathrm{MS_R}$ represents the mean square between subjects, $\mathrm{MS_E}$ represents the residual mean square, and k is the number of repeated measurements.

In this study, ICC values were usually divided into five common intervals: $0 < \mathrm{ICC} \leq 0.25$ indicated poor reliability; $0.25 < \mathrm{ICC} \leq 0.4$ indicated low reliability; $0.4 < \mathrm{ICC} \leq 0.6$ indicated fair reliability; $0.6 < \mathrm{ICC} \leq 0.75$ showed that reliability was good; and $0.75 < \mathrm{ICC} \leq 1.0$ meant that reliability was very good, close to perfect. In practice, we usually expect to have a fair to almost perfect reliability index ($\mathrm{ICC} > 0.4$). In this study, we used the IPCAS and NYU data sets to define intra- (short-term) and inter-session (long-term) test-retest reliability, where scans with short intervals are used to calculate short-term reliability, and scans with long intervals are used to calculate long-term reliability. In addition, since IBA contained only two scans, the two scans were used to calculate intersession reliability.

G. NODE DEFINITION

In this study, a widely used functional parcellation (POWER atlas) was used [29]. The POWER atlas is composed of a set of 264 functional nodes that span the cerebral cortex and subcortical structures. In addition, this atlas divides the 264 subregions into 10 intrinsic connectivity networks (ICNs). The names of the 10 ICNs are indicated in Table 1.

TABLE 1. Definitions of ICNS.

Number	*ICN*	*Number*	*ICN*
ICN1	*motor and somatosensory*	*ICN6*	*frontoparietal*
ICN2	*cingulo-opercular*	*ICN7*	*salience*
ICN3	*auditory*	*ICN8*	*subcortical*
ICN4	*default-mode*	*ICN9*	*ventral attention*
ICN5	*visual*	*ICN10*	*dorsal attention*

III. RESULTS

A. THE DISTRIBUTION OF AE, SE, PE, FE AND PFE

After calculating the entropy of each voxel in the brain, we compared the distribution of the outcomes from the five entropy methods. The two-tailed one-sample T test was performed using entropy maps of the first scan, and the statistical threshold was $p < 0.05$ and cluster size >30 (false discovery rate (FDR) correction). The results are shown in Fig. 2, in which (a), (b), and (c) represent the three data sets. For AE, after correction, the differences among the three data sets were not significant. The other entropy methods showed significant differences.

Next, we extracted the average value of different tissues (gray matter (GM), white matter (WM), and cerebrospinal fluid (CSF)), and one-way ANOVA was performed. Fig. 2 shows the results. As shown in Fig. 3, the five entropy measures were significantly different in different tissues. The AE results showed that the complexity of the WM was significantly higher than that of the GM, and the complexity of the CSF was significantly higher than that of the GM. However, no difference was found between the WM and CSF. The SE was significantly different among the three groups: the complexity of the WM was significantly higher than that of the CSF, and complexity of the CSF was significantly higher than that of the GM. PE showed significant differences among the three groups on the other two data sets; however, there was no difference in the WM and CSF measures found in the IBA data set. For FE, the CSF entropy values were significantly higher than those of the GM and WM, and the GM and WM behaved differently across the different data sets. PFE showed significant differences among the three measures from the three data sets: the complexity of the WM was significantly higher than that of the GM and CSF; the complexity of the GM was significantly higher than that of the CSF.

B. VOXEL-BASED RELIABILITY OF THE FIVE ENTROPY METHODS

Fig. 4 shows the voxel-based test-retest reliability of the five entropy methods on the three data sets. In the figure, the areas where the test-retest reliability was above fair ($\mathrm{ICC} \geq 0.4$) are displayed. Compared with AE, SE had more voxels with fair to good retest reliability, while PE and FE had better test-retest reliability than SE; the reliability of PFE was better than those of the other four entropy methods. In addition,

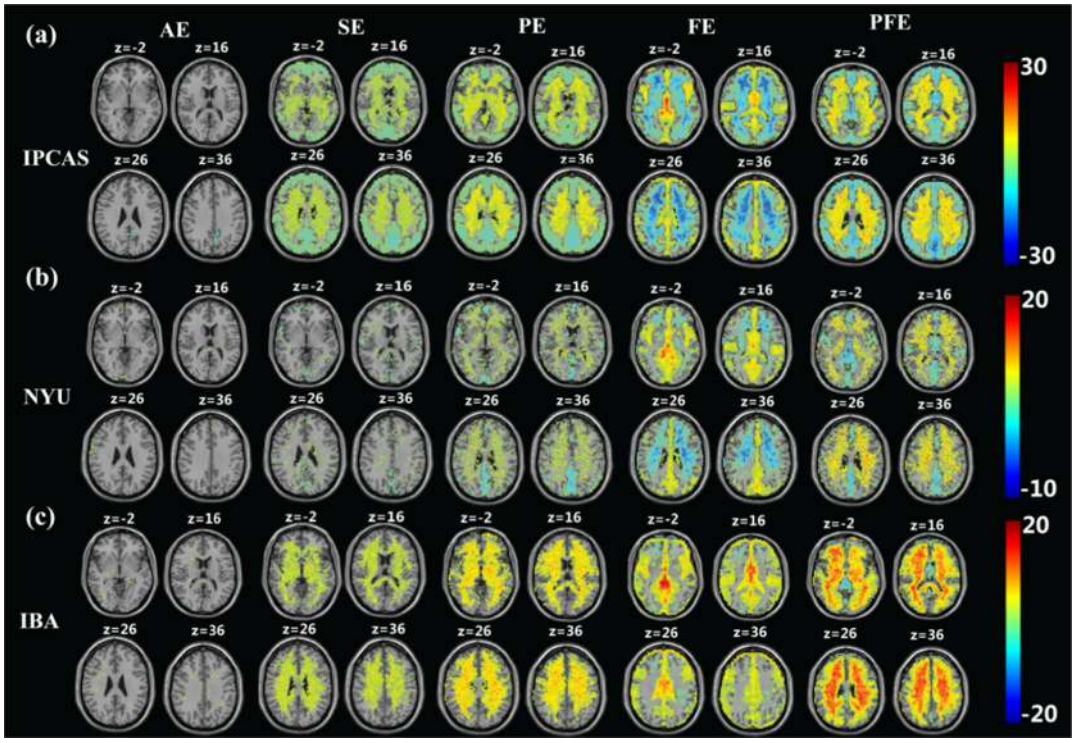

FIGURE 2. One-sample T test results with different entropy methods (FDR correction: $p < 0.05$, cluster size > 30). A, B, and C represent the results from the IPCAS, NYU and IBA data sets, respectively.

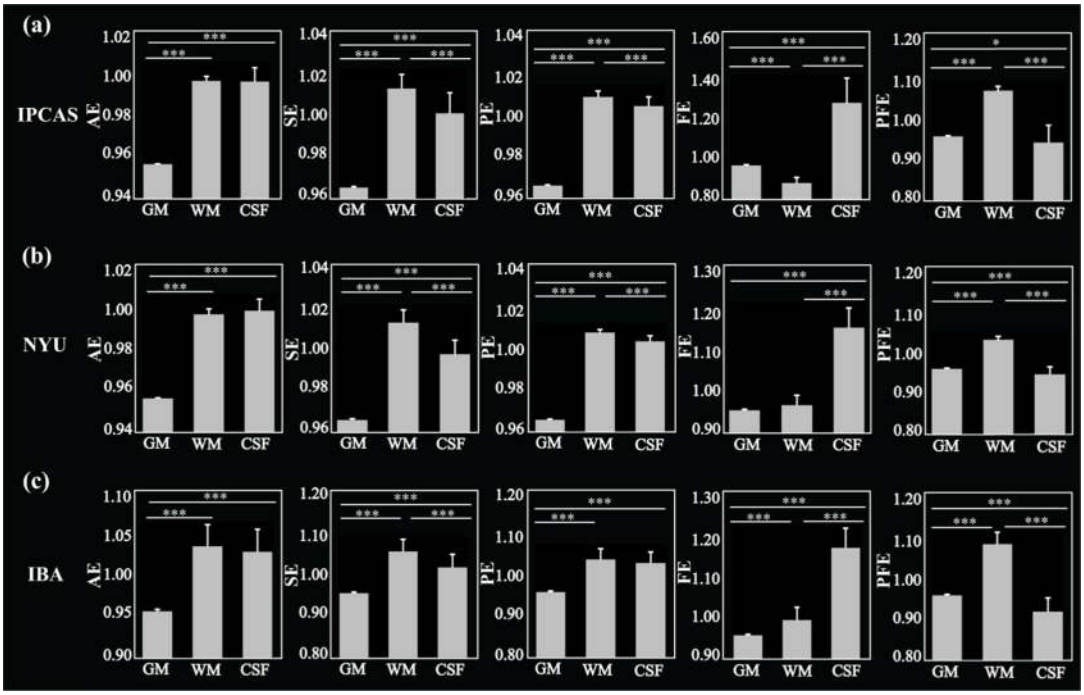

FIGURE 3. Mean entropy values in different tissues. Significant differences between pairs of measures after Bonferroni correction ($p < 0.05$) are indicated. The error bars represent the standard error of entropy values within the group. * indicates $p < 0.05$. ** indicates $p < 0.01$. *** indicates $p < 0.001$.

Fig. 4(a) and Fig. 4(b) show that for the five entropy methods, intra-ICC was better than inter-ICC. Table 2 lists the average ICC of the whole brain for different entropy methods. The three data sets all showed the same trend across the different tissues: AE < SE < FE < PE < PFE.

C. REGION-BASED RELIABILITY OF THE FIVE ENTROPY METHODS

To further study the test-retest reliability of the entropy methods, we extracted the average ICC values of 264 brain regions based on POWER atlas. The results are shown in

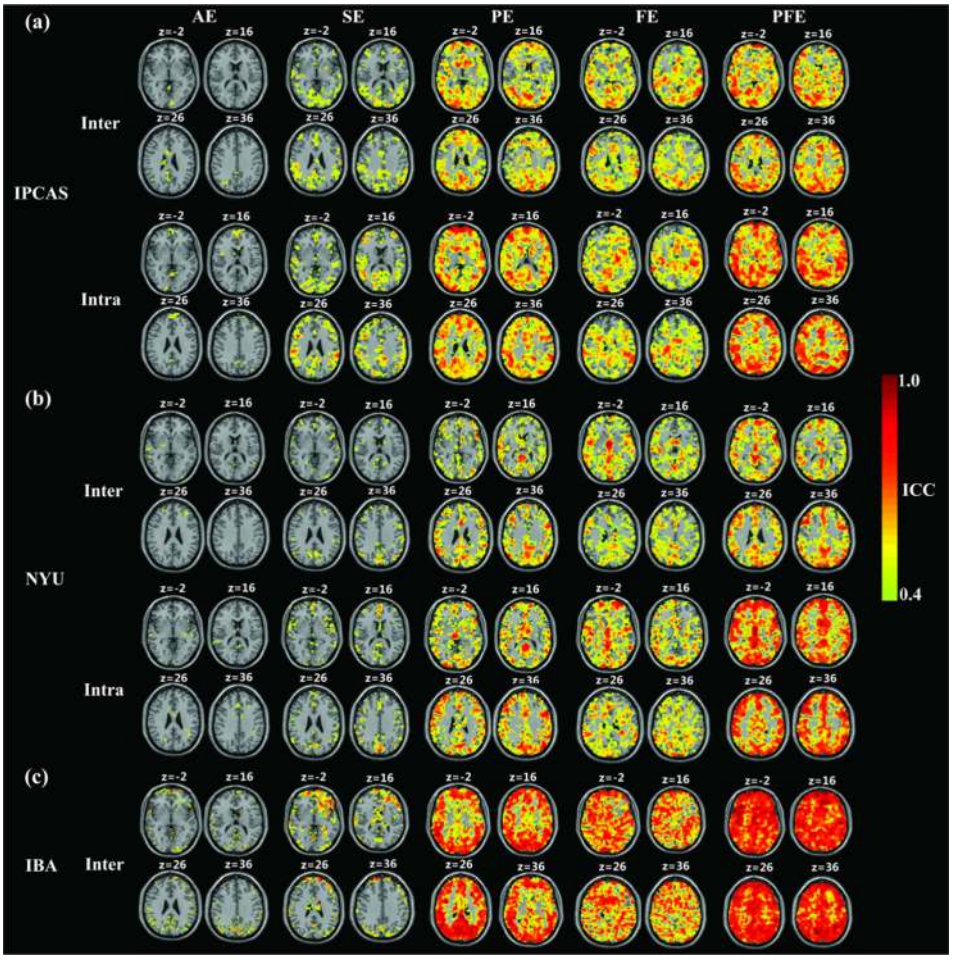

FIGURE 4. Voxel-based test-retest reliability for the five entropy methods with the three data sets. The test-retest reliability that is above fair (ICC ≥ 0.4) is displayed.

TABLE 2. The average ICC of the whole brain for different entropy methods.

	IPCAS		*NYU*		*IBA*
	Inter	*Intra*	*Inter*	*Intra*	*Inter*
AE	*0.1020*	*0.1077*	*0.0895*	*0.1129*	*0.2586*
SE	*0.2240*	*0.2573*	*0.1473*	*0.1952*	*0.3556*
PE	*0.4696*	*0.5778*	*0.4184*	*0.6408*	*0.6773*
FE	*0.2573*	*0.2240*	*0.2304*	*0.3303*	*0.6703*
PFE	*0.3704*	*0.4807*	*0.3655*	*0.5578*	*0.8357*

Fig. 5. We divided the ICC values into 3 intervals: ICC $<$ 0.4 indicates low reliability; 0.4 $\leq$ ICC $<$ 0.6 indicates fair reliability; and ICC $\geq$ 0.6 indicates good reliability. The results showed that, overall, both in short (intra) and long term (inter), AE and SE showed poor to fair reliability, but FE, PE and PFE showed fair to good reliability. PFE in almost all regions presented fair to perfect reliability (ICC $\geq$ 0.4). PE and FE had more brain regions with fair to perfect reliability than AE and SE. It can be seen from the results of Fig. 5(a) and Fig. 5(b) that the test-retest reliability of the intra-session was higher than that of the inter-session analyses.

Fig. 6 shows the percentage of regions under different ICC intervals of the five entropy methods for the three data sets. For the IPCAS data set, the percentage of regions with long-term good to excellent reliability with PFE, PE, FE, SE and AE was 25.38%, 11.36%, 5.31%, 0.38% and 0%, respectively. The percentages of nodes with short-term good to excellent reliability in PFE, FE, PE, SE and AE were 28.78%, 8.33%, 16.67%, 1.52% and 0%, respectively. AE had no brain nodes with inter- or intra-session good to excellent reliability. In addition, better results were obtained with the IBA dataset than with the other two data sets across the five entropy methods, especially for PFE, and the percentage of nodes with fair to excellent reliability was 98.48%.

D. NETWORK-BASED RELIABILITY OF THE FIVE ENTROPY METHODS

Ten functional networks were selected to evaluate the reliability of AE, SE, FE, PE and PFE. The results are shown in Fig. 7. With almost all functional networks, for both intra-session and inter-session analyses, the average ICC values of PFE were higher than those of the other four methods and showed fair to good reliability. PE and FE showed higher reliability than AE and SE. Nevertheless, AE and SE exhibited mean low reliability (mean ICC $<$ 0.3) in all functional networks. In addition, PFE and PE showed fair to good

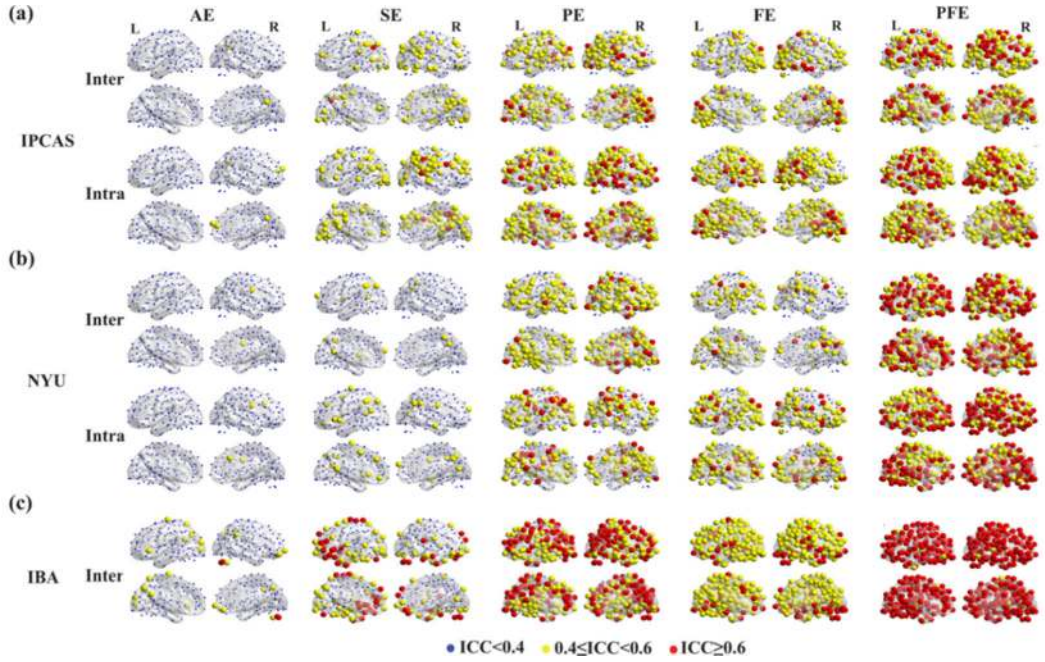

FIGURE 5. Region-based test-retest reliability for the five entropy methods across the three data sets. Nodes with fair to excellent reliability are mapped in yellow ($0.40 \leq ICC < 0.6$) or red ($ICC \geq 0.6$), and those with low reliability ($ICC < 0.4$) are mapped in blue.

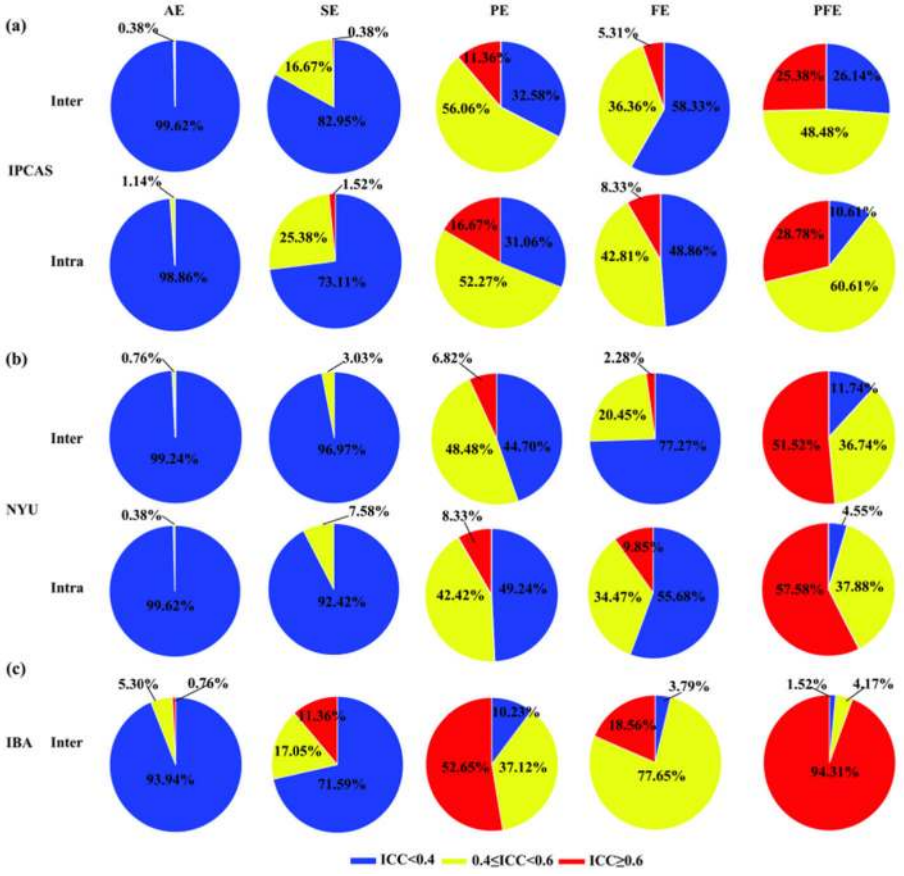

FIGURE 6. Percentage of nodes with different ICC intervals for the five entropy methods across the three data sets.

reliability in the visual network, auditory network, frontoparietal network, default-mode network and ventral attention network.

Finally, we ranked the ICC values of the 264 brain regions from highest to lowest. Table 3 lists the top 10 ranking ICC regions with different entropy methods on the IBA

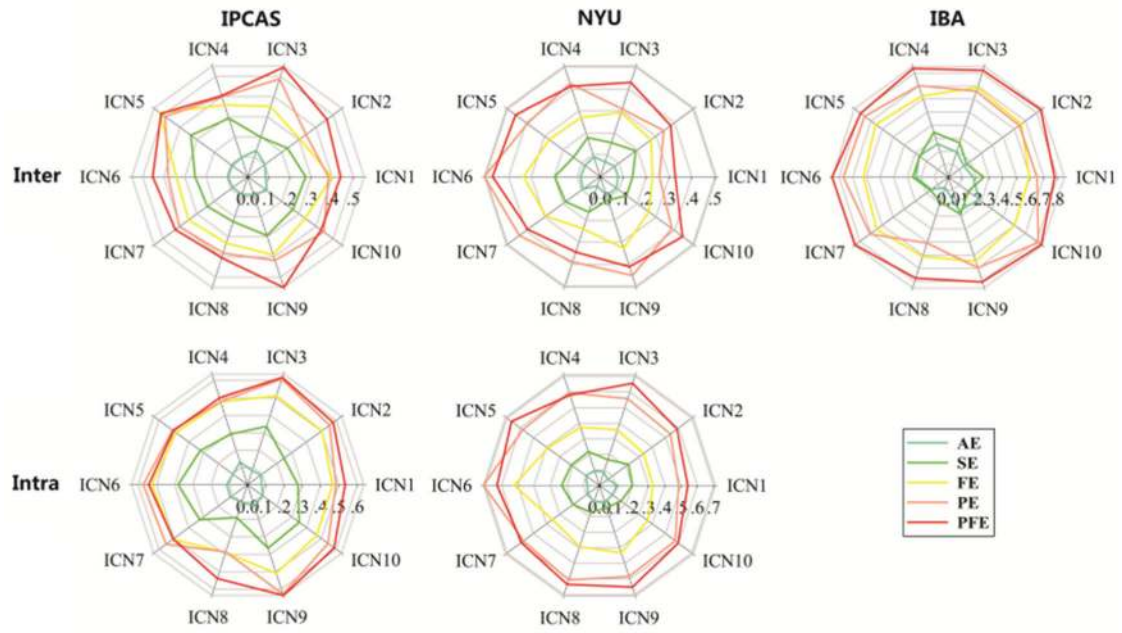

FIGURE 7. Test-retest reliability for the five entropy methods with ten functional networks across the three data sets.

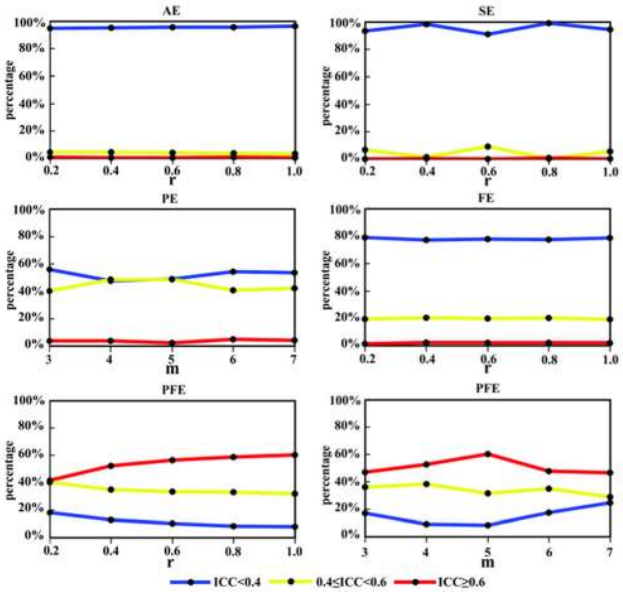

FIGURE 8. Percentage of regions in different ICC intervals for the five entropy methods across all parameter settings.

dataset. Among the top 10 brain regions with high reliability, we found that more than half of the regions were in the default network. The regions identified for the different entropy methods were highly consistent.

E. RELIABILITY OF THE FIVE ENTROPY METHODS WITH DIFFERENT PARAMETERS

We performed the calculations with all possible parameters and compared the test-retest performance of the different entropy methods with these parameter settings. The results are shown in Fig. 8. The results for the five entropy methods are presented as the percentage of nodes in different ICC intervals for the NYU inter-session scans. For AE, SE, FE and PFE, the similarity tolerance r ranged from 0.1 to 1. For PE and PFE, the permuted dimension ranged from 3 to 7. Fig. 8 shows that the different parameters had little effect on the conclusion, and the test-retest reliability of PFE was significantly higher than that of other entropy methods.

IV. DISCUSSION

In this study, three sets of rs-fMRI data were used to map the brain entropy measures using five entropy methods. The tissue distributions and test-retest reliability were studied. The results showed that the entropy measures were very sensitive to the different tissues in the brain. PFE and PE presented fair to perfect test-retest reliability (ICC $\geq$ 0.4) in most regions of the brain; after dividing the brain into 10 functional networks, PFE and PE showed fair to good reliability in the visual network, auditory network, frontoparietal network, default-mode network and ventral attention network. The reliability of entropy methods across the three data sets showed a consistent trend—AE < SE < FE < PE < PFE—and short-term reliability tended to be more stable than long-term reliability.

A. SIGNIFICANT DIFFERENCES IN COMPLEXITY IN THE DIFFERENT BRAIN TISSUES

We mapped whole-brain entropy using rs-fMRI from three data sets. Our data demonstrated that entropy was a sensitive measure for differentiating brain tissues. We performed one-sample T tests with the different brain entropy maps, as shown in Figure 1, and after correction, the difference was not significant for AE. In a previous study, Wang *et al.*

TABLE 3. The top 10 ranking ICC regions with different entropy methods.

	AE		*SE*		*PE*		*FE*		*PFE*	
	MNI	*ICN*	*MNI*	*ICN*	*MNI*	*ICN*	*MNI*	*ICN*	*MNI*	*ICN*
1	*(28, -77, 32)*	*ICN4*	*(28, -77, -32)*	*ICN4*	*(-13, -17, 75)*	*ICN1*	*(28, -77,-32)*	*ICN4*	*(28,-77,-32)*	*ICN4*
2	*(-13, -17, 75)*	*ICN1*	*(6, 67, -4)*	*ICN4*	*(28, -77, -32)*	*ICN4*	*(-51, 8, -2)*	*ICN2*	*(-13,-17,75)*	*ICN1*
3	*(8, 48, -15)*	*ICN4*	*(34, 54, -13)*	*ICN6*	*(-27, -71, 37)*	*ICN10*	*(34, 54, -13)*	*ICN6*	*(-44, 12, -34)*	*ICN4*
4	*(-44, 12, -34)*	*ICN4*	*(8, 48, -15)*	*ICN4*	*(6, -72, 24)*	*ICN5*	*(-13, -17,75)*	*ICN1*	*(-3, 42, 16)*	*ICN4*
5	*(-46, 31, -13)*	*ICN4*	*(-27, -71, 37)*	*ICN10*	*(52, -59, 36)*	*ICN4*	*(52, -2, -16)*	*ICN4*	*(49, 8, -1)*	*ICN2*
6	*(-49, 25,-1)*	*ICN9*	*(-17, -59, 64)*	*ICN10*	*(37, -65, 40)*	*ICN6*	*(-18, -68, 5)*	*ICN5*	*(48, 25, 27)*	*ICN6*
7	*(-16, -46, 73)*	*ICN1*	*(-24, -91, 19)*	*ICN5*	*(15, -63, 26)*	*ICN4*	*(43,-78,-12)*	*ICN5*	*(46, 16, -30)*	*ICN4*
8	*(65, -33, 20)*	*ICN3*	*(-7, -55, 27)*	*ICN4*	*(-2, -37, 44)*	*ICN4*	*(-3, 42, 16)*	*ICN4*	*(-22, 7, -5)*	*ICN8*
9	*(-35, 20, 0)*	*ICN7*	*(-26, -90, 3)*	*ICN5*	*(-24, -91, 19)*	*ICN5*	*(18,-47,-10)*	*ICN5*	*(-10, 55, 39)*	*ICN4*
10	*(65, -12, -19)*	*ICN4*	*(-44, -65, 35)*	*ICN4*	*(47, -50, 29)*	*ICN4*	*(-18, 63, -9)*	*ICN4*	*(-53, 3, -27)*	*ICN4*

calculated the SE map of the whole brain, and consistent with our results, the WM was significantly higher than the mean of the whole brain, and the GM was lower than the mean of the whole brain [30]. Our research results showed that entropy measures applied to fMRI signal complexity analysis had strong tissue sensitivity.

B. COMPARISON OF THE DIFFERENT ENTROPY METHODS

Overall, we found that PFE, PE and FE showed greater reliability with higher ICC values than AE and SE. It can be seen from the calculation formula that both AE and SE can be expressed by the Heaviside function, and the contribution of the Heaviside function depends entirely on the tolerance r and exhibits high sensitivity to changes in r or data point position. Therefore, both AE and SE may significantly change with small changes in the parameter r and may be discontinuous [14], [31]. Regarding FE, after the concept of ''fuzzy set'' was proposed, many studies used ''fuzzy sets'' to measure the similarity of two vectors and used an exponential function as a fuzzy function of FE [32], [33]. According to the rules given by the exponential function, small changes in r do not have much effect on the results. Furthermore, there are no rigid boundaries in the exponential function, and all data points are treated as members. Hence, these factors also mean that the contribution of the exponential function is less sensitive to changes in r and data point position, FE is continuous compared to AE and SE, and FE does not change abruptly when r is slightly changed. These results explain why changes in data point position may have little effect on FE across multiple resting-state scans, thereby producing more reliable results.

In addition, with both AE and SE, vectors are directly formed from the original m consecutive values. Nevertheless, unlike AE and SE, FE uses an m-dimensional vector constructed from a one-dimensional time series [34]. To avoid a short-term physiological change in the time series causing fluctuations in vector coordinates and hiding the similarity between certain vectors, FE promoted the vectors by removing the baseline. Thus, FE can obtain robust estimates with short-term data [35], [36].

PE is different from FE, SE and AE, as it estimates the complexity of a time series through the comparison of neighboring values [37]. In addition, the calculation of PE produces demonstrable time savings [38], and the PE method involves more simplicity and lower complexity in computation without further model assumptions [36], [37], [39], [40]. More notably, all biological systems exhibit linear and nonlinear dynamics, which are subject to interference from external and observational noise [41]. However, compared to other entropy methods, some studies have shown that PE is more robust to existing dynamic and observed noise [42]. Most clinical applications require reliable algorithms over relatively short and noisy time series or over long periods with static- and noise-free data. PE is very reliable for this type of time series, and no further steps are required to preprocess and adjust the parameters [43]. Hence, PE may be more reliable for multiple scans than AE and SE and exhibited higher test-retest reliability.

PFE improved on the antinoise ability of FE by using permutation-based signifying time series. This adaptation enables PFE to effectively restrain the influence caused by noise and is more suitable for capturing information from biological signals. In a previous study, PFE was proven to have better antinoise performance than PE and FE [15]. In this study, our experiments found that PFE had better test-retest reliability than PE and FE.

C. TEST-RETEST RELIABILITY OF THE ENTROPY METHODS

To our knowledge, few studies have focused on analyzing the test-retest reliability of entropy methods based on single-channel time series. One study investigated the ICC of network-wise entropy and found that network-wise complexity for default-mode network exhibited fair reliability (ICC < 0.5) based on eyes-closed sessions [44]. Wang *et al.* calculated SE of fMRI data to evaluate the test-retest stability of SE in normal brain, and the results showed nearly all ICC ≥ 0.5 of intracranial voxels [30]. This finding shows the high reliability of the SE. On the IPCAS and NYU data sets, the reliability of the SE is low to fair, and the fair reliability is presented on the IBA data set (ICC ≥ 0.4). This may be due to different scanning machines and different parameter settings of the machine. This study focuses on the comparison of different entropy methods. On the same data set, the reliability of

PFE is the best, and other entropy methods are still effective indicators.

D. TEST-RETEST RELIABILITY OF INTER-SESSION AND INTRA-SESSION ANALYSES

Many studies have reported the inter-session and intra-session reliability of rs-fMRI signals [44], [45]. In this paper, we observed that intra-session analyses showed higher test-retest reliability than inter-session analyses with the five entropy methods. This finding was consistent with previous findings that the spatial patterns of functional networks had higher reliability in short-term scans [45]. Wang *et al.* also found that the ICC values with the default-mode network in intra-session scans were higher than those in intersession scans based on network-wise entropy [44]. This finding may suggest that short-term scans may have reduced internal noise with improved reliability estimates and that short-term scanning intervals can result in more stable and accurate entropy values [46].

E. FUNCTIONAL NETWORK RELIABILITY IN THE RESTING STATE

Our research results showed that the test-retest reliability of PFE and PE was fair to good on almost all functional networks. As seen in Fig.7., across both intra-session and inter-session analyses, the reliability values for the ventral attention, visual, auditory and frontoparietal networks were relatively stable and relatively higher than in other networks.

The ventral attention network is composed of the right lateral temporoparietal junction (TPJ) and the ventral frontal cortex (VFC) and participates in the bottom-up processing of attentional reorientation [47]. This network shows activity increases upon detection of salient targets, especially when they appear in unexpected locations [48]. Of note, the most important factor in the visual network is sensing the physical metrics of the spatial layout [49], and the auditory network is primarily active when external stimuli are received [50]. In addition, the frontoparietal network can maintain control signals online in working memory from one or a small number of trials to the next, enabling it to implement task control on a faster trial-to-trial basis [51]. Nevertheless, in the resting state, the subjects were not disturbed by the outside world, and therefore, few stimuli were present during the resting state regarding the construction of these networks. Hence, these networks may not be active, which corresponded to fewer changes in complexity. In other words, due to less activity, these networks were relatively stable and robust in the resting state.

The regions with perfect reliability were predominantly distributed in the default-mode network. Usually, when the individual is not focused on the outside world in the resting state, the default-mode network will be very active [52]. The default-mode network has been suggested to be responsible for mind wandering during the resting state. The default-mode network was reported as a main functional system in the human brain [53]. Especially for the intra-session scans, the default-mode network is synchronously activated, which could result in some brain regions in the default network showing high test-retest reliability.

V. CONCLUSION

In summary, we studied the distribution and test-retest reliability of the measures from five entropy methods derived from rs-fMRI data. Specifically, our research found that entropy has strong tissue sensitivity, and all entropy methods showed significant differences in different brain tissues (GM, WM and CSF). We used 3 data sets and found that the reliability of PFE was optimal, followed by PE and FE, at three levels (i.e., based on voxels, brain regions, and functional networks). The results showed overall fair to perfect reliability for PFE and FE. Our results demonstrated that PFE and PE were more reliable and stable for complexity analyses of fMRI signals, providing methodological guidance for exploring brain activity by fMRI signals.

VI. LIMITATIONS

There are still some limitations in our research. First, we studied some commonly used entropy measures; however, many improvements in these methods have not yet been explored. We propose further studies on the test-retest reliability of complexity methods. Second, in this study, we mainly studied the test-retest reliability of different entropy methods and chose the widely used POWER atlas; however, other atlases can also be considered.

ACKNOWLEDGMENT

(Yan Niu and Jie Sun are co-first authors.) Thanks to Bin Wang, Waqar Hussain, Chanjuan Fan, Rui Cao, Mengni Zhou, and Jie Xiang for their suggestions and guidance on this research.

REFERENCES

[1] C. Coronel, H. Garn, M. Waser, M. Deistler, T. Benke, P. Dal-Bianco, G. Ransmayr, S. Seiler, D. Grossegger, and R. Schmidt, "Quantitative EEG markers of entropy and auto mutual information in relation to MMSE scores of probable Alzheimer's disease patients," *Entropy*, vol. 19, no. 3, p. 130, Mar. 2017.

[2] J. Monge, C. Gómez, J. Poza, A. Fernández, J. Quintero, and R. Hornero, "MEG analysis of neural dynamics in attention-deficit/hyperactivity disorder with fuzzy entropy," *Med. Eng. Phys.*, vol. 37, no. 4, pp. 416–423, Apr. 2015.

[3] J. Sun, B. Wang, Y. Niu, Y. Tan, C. Fan, N. Zhang, J. Xue, J. Wei, and J. Xiang, "Complexity analysis of EEG, MEG, and fMRI in mild cognitive impairment and Alzheimer's disease: A review," *Entropy*, vol. 22, no. 2, p. 239, Feb. 2020.

[4] N. K. Logothetis, J. Pauls, M. Augath, T. Trinath, and A. Oeltermann, "Neurophysiological investigation of the basis of the fMRI signal," *Nature*, vol. 412, no. 6843, pp. 150–157, Jul. 2001.

[5] R. Ju, C. Hu, P. Zhou, and Q. Li, "Early diagnosis of Alzheimer's disease based on resting-state brain networks and deep learning," *IEEE/ACM Trans. Comput. Biol. Bioinf.*, vol. 16, no. 1, pp. 244–257, Jan. 2019.

[6] T. V. Yakovleva, I. E. Kutepov, A. Y. Karas, N. M. Yakovlev, V. V. Dobriyan, I. V. Papkova, M. V. Zhigalov, O. A. Saltykova, A. V. Krysko, T. Y. Yaroshenko, N. P. Erofeev, and V. A. Krysko, "EEG analysis in structural focal epilepsy using the methods of nonlinear dynamics (Lyapunov exponents, Lempel-Ziv complexity, and multiscale entropy)," *Sci. World J.*, vol. 2020, pp. 1–13, Feb. 2020.

[7] Z. Ali, M. S. Hossain, G. Muhammad, and M. Aslam, "New zero-watermarking algorithm using hurst exponent for protection of privacy in telemedicine," *IEEE Access*, vol. 6, pp. 7930–7940, Jan. 2018.

[8] R. X. Smith, L. Yan, and D. J. J. Wang, "Multiple time scale complexity analysis of resting state FMRI," *Brain Imag. Behav.*, vol. 8, no. 2, pp. 284–291, Jun. 2014.

[9] N. K. Al-Qazzaz, S. Ali, S. A. Ahmad, M. S. Islam, and J. Escudero, "Entropy-based markers of EEG background activity of stroke-related mild cognitive impairment and vascular dementia patients," in *Proc. SEIA*, Barcelona., Spain, 2016, pp. 92–94.

[10] J. M. Yentes, N. Hunt, K. K. Schmid, J. P. Kaipust, D. McGrath, and N. Stergiou, "The appropriate use of approximate entropy and sample entropy with short data sets," *Ann. Biomed. Eng.*, vol. 41, no. 2, pp. 349–365, Feb. 2013.

[11] J. S. Richman, D. E. Lake, and J. R. Moorman, "Sample entropy," *Methods Enzymol.*, vol. 384, pp. 172–184, Jan. 2004.

[12] W. Chen, Z. Wang, H. Xie, and W. Yu, "Characterization of surface EMG signal based on fuzzy entropy," *IEEE Trans. Neural Syst. Rehabil. Eng.*, vol. 15, no. 2, pp. 266–272, Jun. 2007.

[13] C. Bandt and B. Pompe, "Permutation entropy: A natural complexity measure for time series," *Phys. Rev. Lett.*, vol. 88, no. 17, Apr. 2002, Art. no. 174102.

[14] J. S. Richman and J. R. Moorman, "Physiological time-series analysis using approximate entropy and sample entropy," *Amer. J. Physiol.-Heart Circulatory Physiol.*, vol. 278, no. 6, pp. H2039–H2049, Jun. 2000.

[15] Y. Niu, R. Cao, H. Wang, C. Li, M. Zhou, Y. Guo, B. Wang, P. Yan, and J. Xiang, "Permutation fuzzy entropy—An index for the analysis of epileptic electroencephalogram," *J. Med. Imag. Health Informat.*, vol. 9, no. 3, pp. 637–645, Mar. 2019.

[16] M. O. Sokunbi, R. T. Staff, G. D. Waiter, G. G. Cameron, and A. D. Murray, "Functional MRI entropy measurements of age-related brain changes," in *Proc. 17th Annu. Meeting Org. Hum. Brain Mapping*, Quebec City, QC, Canada, Jun. 2011.

[17] M. O. Sokunbi, V. B. Gradin, G. D. Waiter, G. G. Cameron, T. S. Ahearn, A. D. Murray, D. J. Steele, and R. T. Staff, "Nonlinear complexity analysis of brain fMRI signals in schizophrenia," *PLoS ONE*, vol. 9, no. 5, May 2014, Art. no. e95146.

[18] M. O. Sokunbi, W. Fung, V. Sawlani, S. Choppin, D. E. J. Linden, and J. Thome, "Resting state fMRI entropy probes complexity of brain activity in adults with ADHD," *Psychiatry Res., Neuroimaging*, vol. 214, no. 3, pp. 341–348, Dec. 2013.

[19] M. O. Sokunbi, G. G. Cameron, T. S. Ahearn, A. D. Murray, and R. T. Staff, "Fuzzy approximate entropy analysis of resting state fMRI signal complexity across the adult life span," *Med. Eng. Phys.*, vol. 37, no. 11, pp. 1082–1090, Nov. 2015.

[20] C. Lin, S.-H. Lee, C.-M. Huang, G.-Y. Chen, P.-S. Ho, H.-L. Liu, Y.-L. Chen, T. M.-C. Lee, and S.-C. Wu, "Increased brain entropy of resting-state fMRI mediates the relationship between depression severity and mental health-related quality of life in late-life depressed elderly," *J. Affect. Disorders*, vol. 250, pp. 270–277, May 2019.

[21] X.-W. Song, Z.-Y. Dong, X.-Y. Long, S.-F. Li, X.-N. Zuo, C.-Z. Zhu, Y. He, C.-G. Yan, and Y.-F. Zang, "REST: A toolkit for resting-state functional magnetic resonance imaging data processing," *PLoS ONE*, vol. 6, no. 9, Sep. 2011, Art. no. e25031.

[22] C. G. Yan, X. D. Wang, X. N. Zuo, and Y. F. Zang, "DPABI: Data processing & analysis for (resting-state) brain imaging," *Neuroinformatics*, vol. 14, no. 3, pp. 339–351, Jul. 2016.

[23] A. Schultz, M. Siedenberg, U. Grouven, T. Kneif, and B. Schultz, "Comparison of narcotrend index, bispectral index, spectral and entropy parameters during induction of propofol-remifentanil anaesthesia," *J. Clin. Monitor. Comput.*, vol. 22, no. 2, pp. 103–111, Apr. 2008.

[24] L. Tocado, E. Palacios, and R. Burriel, "Entropy determinations and magnetocaloric parameters in systems with first-order transitions: Study of MnAs," *J. Appl. Phys.*, vol. 105, no. 9, pp. 722–724, May 2009.

[25] J. Li, J. Yan, X. Liu, and G. Ouyang, "Using permutation entropy to measure the changes in EEG signals during absence seizures," *Entropy*, vol. 16, no. 6, pp. 3049–3061, May 2014.

[26] J. B. Williams, M. Gibbon, M. B. First, R. L. Spitzer, M. Davies, J. Borus, and H. U. Wittchen, "The structured clinical interview for DSM-III-R (SCID): II. Multisite test-retest reliability," *Arch. Gen. Psychiatry*, vol. 49, no. 8, pp. 630–636, Aug. 1992.

[27] K. Rongsawad, L. Worawan, K. Jirarojprapa, S. Kaewkham, and S. Khattiwong, "72 test-retest reliability and minimal detectable change for postural sway by using sway meter in elderly subjects," *Age Ageing*, vol. 48, pp. iv18–iv27, Dec. 2019.

[28] W. J. Chambers, J. Puig-Antich, M. Hirsch, P. Paez, P. J. Ambrosini, M. A. Tabrizi, and M. Davies, "The assessment of affective disorders in children and adolescents by semistructured interview. Test-retest reliability of the schedule for affective disorders and schizophrenia for school-age children, present episode version," *Arch Gen Psychiatry*, vol. 42, no. 7, pp. 696–702, Jul. 1985.

[29] J. D. Power, A. L. Cohen, S. M. Nelson, G. S. Wig, K. A. Barnes, J. A. Church, A. C. Vogel, T. O. Laumann, F. M. Miezin, B. L. Schlaggar, and S. E. Petersen, "Functional network organization of the human brain," *Neuron*, vol. 72, no. 4, pp. 665–678, Nov. 2011.

[30] Z. Wang, Y. Li, A. R. Childress, and J. A. Detre, "Brain entropy mapping using fMRI," *PLoS ONE*, vol. 9, no. 3, Mar. 2014, Art. no. e89948.

[31] S. M. Pincus, "Approximate entropy as a measure of system complexity," *Proc. Nat. Acad. Sci. USA*, vol. 88, pp. 2297–2301, Mar. 1991.

[32] Z. Cao and C.-T. Lin, "Inherent fuzzy entropy for the improvement of EEG complexity evaluation," *IEEE Trans. Fuzzy Syst.*, vol. 26, no. 2, pp. 1032–1035, Apr. 2018.

[33] J.-M. Girault and A. Humeau-Heurtier, "Centered and averaged fuzzy entropy to improve fuzzy entropy precision," *Entropy*, vol. 20, no. 4, p. 287, Apr. 2018.

[34] S. He, K. Sun, and R. Wang, "Fractional fuzzy entropy algorithm and the complexity analysis for nonlinear time series," *Eur. Phys. J. Special Topics*, vol. 227, nos. 7–9, pp. 943–957, Oct. 2018.

[35] C. Lohrmann, P. Luukka, M. Jablonska-Sabuka, and T. Kauranne, "A combination of fuzzy similarity measures and fuzzy entropy measures for supervised feature selection," *Expert Syst. Appl.*, vol. 110, pp. 216–236, Nov. 2018.

[36] J. Xiang, C. Li, H. Li, R. Cao, B. Wang, X. Han, and J. Chen, "The detection of epileptic seizure signals based on fuzzy entropy," *J. Neurosci. Methods*, vol. 243, pp. 18–25, Mar. 2015.

[37] M. Zanin, L. Zunino, O. A. Rosso, and D. Papo, "Permutation entropy and its main biomedical and econophysics applications: A review," *Entropy*, vol. 14, no. 8, pp. 1553–1577, Aug. 2012.

[38] K. Kuntzelman, L. Jack Rhodes, L. N. Harrington, and V. Miskovic, "A practical comparison of algorithms for the measurement of multiscale entropy in neural time series data," *Brain Cognition*, vol. 123, pp. 126–135, Jun. 2018.

[39] F. Taherkhani, M. Rahmani, F. Taherkhani, H. Akbarzadeh, and H. Abroshan, "Permutation entropy and detrend fluctuation analysis for the natural complexity of cardiac heart interbeat signals," *Phys. A, Stat. Mech. Appl.*, vol. 392, no. 14, pp. 3106–3112, Jul. 2013.

[40] C. Bandt, "A new kind of permutation entropy used to classify sleep stages from invisible EEG microstructure," *Entropy*, vol. 19, no. 5, p. 197, Apr. 2017.

[41] X. Li, S. Cui, and L. J. Voss, "Using permutation entropy to measure the electroencephalographic effects of sevoflurane," *Anesthesiology*, vol. 109, no. 3, pp. 448–456, Sep. 2008.

[42] F. Traversaro, W. Legnani, and F. O. Redelico, "Influence of the signal to noise ratio for the estimation of permutation entropy," *Phys. A, Stat. Mech. Appl.*, vol. 553, Sep. 2020, Art. no. 124134.

[43] B. Deng, L. Cai, S. Li, R. Wang, H. Yu, Y. Chen, and J. Wang, "Multivariate multi-scale weighted permutation entropy analysis of EEG complexity for Alzheimer's disease," *Cognit. Neurodyn.*, vol. 11, pp. 217–231, Jun. 2017.

[44] X. Wang, Y. Jiao, T. Tang, H. Wang, and Z. Lu, "Investigating univariate temporal patterns for intrinsic connectivity networks based on complexity and low-frequency oscillation: A test-retest reliability study," *Neuroscience*, vol. 254, pp. 404–426, Dec. 2013.

[45] X.-N. Zuo and X.-X. Xing, "Test-retest reliabilities of resting-state FMRI measurements in human brain functional connectomics: A systems neuroscience perspective," *Neurosci. Biobehavioral Rev.*, vol. 45, pp. 100–118, Sep. 2014.

[46] Q. Zou, X. Long, X. Zuo, C. Yan, C. Zhu, Y. Yang, D. Liu, Y. He, and Y. Zang, "Functional connectivity between the thalamus and visual cortex under eyes closed and eyes open conditions: A resting-state fMRI study," *Human Brain Mapping*, vol. 30, no. 9, pp. 3066–3078, Sep. 2009.

[47] K. Farrant and L. Q. Uddin, "Asymmetric development of dorsal and ventral attention networks in the human brain," *Develop. Cognit. Neurosci.*, vol. 12, pp. 165–174, Apr. 2015.

[48] H. Kim, "Involvement of the dorsal and ventral attention networks in oddball stimulus processing: A meta-analysis: Oddball stimulus processing," *Hum. Brain Mapping*, vol. 35, no. 5, pp. 2265–2284, May 2014.

[49] A. Harel, D. J. Kravitz, and C. I. Baker, "Deconstructing visual scenes in cortex: Gradients of object and spatial layout information," *Cerebral Cortex*, vol. 23, no. 4, pp. 947–957, Apr. 2013.

[50] D. M. Torta, F. A. Jure, O. K. Andersen, and J. A. B. B. Manresa, "Intense and sustained pain reduces cortical responses to auditory stimuli: Implications for the interpretation of the effects of heterotopic noxious conditioning stimulation in humans," *Eur. J. Neurosci.*, vol. 50, no. 12, pp. 3934–3943, Dec. 2019.
[51] E. L. Johnson, D. King-Stephens, P. B. Weber, K. D. Laxer, J. J. Lin, and R. T. Knight, "Spectral imprints of working memory for everyday associations in the frontoparietal network," *Frontiers Syst. Neurosci.*, vol. 12, p. 65, Jan. 2019.
[52] A. Duarte, "Musement: The activity of the brain's default mode network," *Semiotica*, vol. 2020, no. 233, pp. 145–158, Mar. 2020.
[53] T. Meindl, S. Teipel, R. Elmouden, S. Müeller, W. Koch, O. Dietrich, U. Coates, M. Reiser, and C. Glaser, "Test-retest reproducibility of the default-mode network in healthy individuals," *Hum. Brain Mapping*, vol. 31, no. 2, pp. 237–246, Feb. 2010.

YAN NIU is currently pursuing the Ph.D. degree with the College of Information and Computer, Taiyuan University of Technology, Taiyuan, China. She is also a Certified Senior Software Engineer. She is major in computer application technology. She has published more than 17 articles. Her research interests include exploration of nonlinear dynamics methods, study of functional magnetic resonance signal complexity, and early diagnosis of Alzheimer's disease.

JIE SUN received the B.S. degree from the Taiyuan University of Technology, where she is currently pursuing the master's degree. She is majoring in computer science and technology research, with a focus on intelligent information processing, brain non-linear analysis, and machine learning. She is also a Certified Middle Software Engineer. Her research interests include improving detection of Alzheimer's disease and known brain complexity changes during aging. Her awards and honors include third-level computing.

BIN WANG received the Ph.D. degree from Okayama University, Japan, in 2013. He is currently an Associate Professor with the School of Information and computer Science and Technology, Taiyuan University of Technology. His research interests include study of brain cognitive function and the diagnosis of mental diseases.

WAQAR HUSSAIN received the B.S. degree in computer science from the University of Azad Jammu and Kashmir, Muzaffarabad Azad Kashmir, Pakistan, in 2006, and the M.S. degree from the Department of Computer Science, Muhammad Ali Jinnah University Islamabad, Pakistan, in 2011. He is currently pursuing the Ph.D. degree with the College of Information and Computing, Taiyuan University of Technology, Taiyuan, China. He is major in computer application technology. His research interests include biomedical signal processing, deep learning, machine learning, and pattern learning.

CHANJUAN FAN is currently pursuing the master's degree with the Taiyuan University of Technology. She is major in computer science and technology. Her research interests include brain science and intelligent computing, specifically on brain networks, brain dynamics, and lesions.

RUI CAO received the Ph.D. degree in computer application technology from the Taiyuan University of Technology. He is currently an Associate Professor with the Software College, Taiyuan University of Technology. His research interests include brain science and intelligent information processing.

MENGNI ZHOU is currently pursuing the Ph.D. degree with the Graduate School of Interdisciplinary Science and Engineering in Health Systems, Okayama University. She has published five articles. She is currently conducting research in cognitive neuroscience. Her research interest includes EEG signal analysis based on deep learning.

JIE XIANG received the M.S. and Ph.D. degrees in computer science and technology from the Taiyuan University of Technology. She is currently a Professor and a Ph.D. Supervisor with the College of Information and Computer, Taiyuan University of Technology. Her research interests include brain science and intelligent computing, intelligent information processing, and big data management and analysis.